JOURNAL OF SOLID STATE CHEMISTRY 72, 272–282 (1988)

Vibrational Study of Metal-Substituted MPS_3 Layered Compounds: $M^{II}_{1-x}M^{I}_{2x}PS_3$ with M^{II} = Mn, Cd, and M^{I} = Cu (x = 0.13) or Ag (x = 0.50)

I. Comprehensive Infrared and Raman Analysis and Structural Properties

O. POIZAT*

LASIR, CNRS, 2 rue Henri Dunant, 94320 Thiais, France

C. SOURISSEAU

Laboratoire de Spectroscopie Moléculaire et Cristalline, UA 124, CNRS, Université de Bordeaux I, 33405 Talence, France

AND Y. MATHEY

Laboratoire de Spectrochimie des Eléments de Transition, UA 420, Université Paris-Sud, 91405 Orsay, France

Received February 18, 1987

The infrared, polarized Raman, and inelastic neutron scattering spectra (650–10 cm^{-1}) of $M^{II}_{0.87}Cu^{I}_{0.26}PS_3$ and $M^{II}_{0.5}Ag^{I}_{1.0}PS_3$ compounds, where M^{II} = Mn, Cd, have been recorded and compared with those of the related $M^{II}PS_3$ derivatives. It is shown that all these new metal-substituted systems maintain a bidimensional structure ($CdCl_2$ type) consisting of $P_2S_6^{4-}$ entities, monometallic $M^{II}S_6$, and bimetallic $(M^{I})_2S_6$ octahedra. The copper derivatives are disordered because of a random distribution of Cu_2S_6 entities; meanwhile, the silver-containing lattices seem ordered. The vibrational modes assigned to translational motions of Cu^{I} and Ag^{I} cations have been clearly identified in the low-frequency region ($\nu < 75\ cm^{-1}$). Finally, the magnetic and vibrational properties of the $Mn_{0.87}Cu_{0.26}PS_3$ host lattice intercalated with $Co(C_5H_5)_2^+$ have been investigated; this definitely confirms the layered character of this new family of compounds. © 1988 Academic Press, Inc.

Introduction

The two-dimensional $M^{II}PS_3$ phases, where M^{II} is a transition metal ion, are known to intercalate guest molecules or ions (*1–3*) and to exhibit interesting electrical (*3–5*) and magnetic properties (*3–6*). For a long time, only $FePS_3$ has been the subject of full X-ray structural determinations (*7*) but recently accurate crystal structures of several MPS_3 phases have been established (*8–13*). Their structure is related to that of $CdCl_2$, with metal ions and phosphorus–phosphorus (P–P) pairs occupying

* To whom correspondence should be addressed.

0022-4596/88 $3.00

Copyright © 1988 by Academic Press, Inc.
All rights of reproduction in any form reserved.

the cadmium positions and sulfur occupying the chloride positions; the metal ions and P–P pairs are approximately octahedrally coordinated in a distorted cubic close-packed lattice and the monoclinic structures result from the stacking of $SM^{II}_{2/3}(P_2)_{1/3}S$ slabs developed in the $(a \times b)$ planes and separated by van der Waals gaps.

In a preliminary communication (*14*), we reported the preparation and a survey of the structural, vibrational, and conduction properties of a new class of layer-type MPS_3 compounds, $M^{II}_{1-x}M^{I}_{2x}PS_3$ where M^I = Cu (x = 0.13) or Ag (x = 0.5). We concluded that these new materials come from partial substitution of the M^{II} ions within the layers and that the Cu^I ions are involved in a dynamic process responsible for the ionic conduction properties. Then, a complete structural determination of $Mn_{0.87}Cu_{0.26}PS_3$ was established from single-crystal X-ray diffraction and powder EXAFS measurements (*15*). It turned out that in this lattice 13% of the Mn^{II} ions are randomly substituted by bimetallic $(Cu^I)_2$ pairs. The distorted layers thus contain (P_2S_6), (MnS_6), and ($S_3Cu \ldots CuS_3$) pseudooctahedra and they are still separated by empty van der Waals gaps. Consequently, these materials may behave as potential new host structures for intercalation reactions.

The opportunity to obtain new host materials in conjunction with interesting conductivity properties led us to carry out additional preparative and spectroscopic studies on other metal-substituted MPS_3 phases, in particular, the above-mentioned $Mn_{0.5}Ag_{1.0}PS_3$ compound and the related cadmium derivatives, $Cd_{0.87}Cu_{0.26}PS_3$ and $Cd_{0.5}Ag_{1.0}PS_3$. Unfortunately, no single crystals suitable for X-ray studies were obtained in the latter cases and their detailed structures are still open to discussion. Nevertheless, much structural and dynamic information can be obtained from vibrational studies as emphasized in some previous work devoted to $M^{II}PS_3$ (*16–20*) and $Cr^{III}_{0.5}M^{I}_{0.5}PS_3$ (*21*) compounds.

We have thus carried out an extensive vibrational study of the title compounds to compare the structures of $Mn_{0.5}Ag_{1.0}PS_3$, $Cd_{0.87}Cu_{0.26}PS_3$, and $Cd_{0.5}Ag_{1.0}PS_3$ with that of $Mn_{0.87}Cu_{0.26}PS_3$. This paper reports a comprehensive infrared and Raman study and some incoherent inelastic neutron scattering investigations of these phases and of the intercalated $Mn_{0.70}Cu_{0.26}PS_3$, $[Co(C_5H_5)_2]_{0.34}$ system. The accompanying paper (*22*) deals with a temperature-dependent analysis of the low-frequency vibrational spectra, providing better insight into possible ionic transport mechanisms.

Experimental

Synthesis

The syntheses of polycrystalline $Mn_{0.87}Cu_{0.26}PS_3$ and $Mn_{0.5}Ag_{1.0}PS_3$ from appropriate amounts of the pure elements have already been described (*14, 15*); $Cd_{0.87}Cu_{0.26}PS_3$ and $Cd_{0.5}Ag_{1.0}PS_3$ were obtained using the same procedure. The purity of the samples was checked by chemical analysis and powder X-ray diffraction methods; the observed stoichiometries correspond to the maximum degrees of metal substitution experimentally reached. However, less substituted phases, with $0 < x < 0.13$ for Cu^I and $0 < x < 0.5$ for Ag^I, could also be prepared by decreasing the M^I content in the reaction mixtures. Subsequent treatment by chemical transport yields the formation of single crystals of various qualities: $Mn_{0.87}Cu_{0.26}PS_3$ forms thin platelets (ca. $1.0 \times 3.0 \times 4.0$ mm^3) parallel to the layer planes (**a**, **b**), making it possible to record polarized Raman spectra and to perform infrared absorption and reflection measurements (see below); alternatively, $Mn_{0.5}Ag_{1.0}PS_3$ and $Cd_{0.87}Cu_{0.26}PS_3$ form conglomerates with rough and overlapping

crystalline faces (ca. 0.2 × 0.2 mm^2 and 1.0 × 2.0 mm^2, respectively) suitable for polarized Raman experiments. Finally, single crystals of $Cd_{0.5}Ag_{1.0}PS_3$ were never obtained. Intercalation of $Mn_{0.87}Cu_{0.26}PS_3$ has been performed by treating the host material with alcoholic solutions of $(C_5H_5)_2CoI$, according to the method described in Ref. (*23*). From elemental analysis, this reaction leads to the stoichiometry $Mn_{0.87-y/2}Cu_{0.26}PS_3$, $[Co(C_5H_5)_2]_y$, where y = 0.34.

Physical Measurements

First, XPS and Auger spectra were recorded at 240 K on polycrystalline samples of $Mn_{0.87}Cu_{0.26}PS_3$ to check that neither Cu^{II} nor Cu^0 centers were present (*24*). The Raman spectra were obtained on a triple monochromator Dilor RTI30 instrument using the 514.5-nm line of a Spectra Physics Model 164 Ar^+ laser; weak exciting intensities were generally used, ca. 100 mW for powder samples and ca. 5 mW for single crystals.

Infrared spectra were recorded on a Perkin–Elmer 983 spectrometer (4000–200 cm^{-1}), and on a Brucker IFS 113V interferometer (300–20 cm^{-1}). Powder samples were dispersed in Nujol for absorption measurements or pressed into pure pellets for reflection analyses. Absorption and reflection experiments on crystalline platelets, using the configuration **E** parallel to the (*ab*) layer planes, were carried out with a beam condenser (8×) and all the reflection spectra were obtained at near-normal incidence (~10°).

Inelastic neutron scattering (INS) experiments were performed at the Institut Laue Langevin (ILL, Grenoble, France) on the focusing IN6 time-of-flight spectrometer using an incident wavelength of 5.9 Å and covering the 0.245–1.734 $Å^{-1}$ range of momentum transfer. The powder sample $Mn_{0.87}Cu_{0.26}PS_3$ was contained in a circular slab-shaped aluminum container (ϕ = 5 cm) and its thickness was adjusted to ensure a transmission better than 90% to minimize multiscattering processes. The data reduction program CROSSX (*25*) was used to calculate the incoherent scattering law $S_{inc}(\alpha, \beta)$, where $\alpha = hQ^2/2kTM$, $\beta = hw/kT$. To compare INS results with optical data, the frequency distribution function

$$\rho(\beta) = 2\beta \sinh \beta/2 \left[\lim_{\alpha \to 0} \frac{S(\alpha, \beta)}{\alpha}\right]$$

was calculated using the extrapolation procedure (*26*) performed with the program Florence at the ILL.

Finally, the magnetic susceptibility measurements were performed with use of the Faraday method between 402 and 300 K. The χ_M^{-1}-versus-temperature curves strongly resemble the behavior observed in $MnPS_3$ intercalates (*27, 28*).

Results and Discussion

Vibrational Spectra of the $M^{II}_{1-x}M^{I}_{2x}PS_3$ Compounds

In Fig. 1, one can compare the infrared absorption and Raman scattering spectra (650–10 cm^{-1}) of $MnPS_3$, $Mn_{0.87}Cu_{0.26}PS_3$, and $Mn_{0.5}Ag_{1.0}PS_3$ and of $CdPS_3$, $Cd_{0.87}Cu_{0.26}PS_3$, and $Cd_{0.5}Ag_{1.0}PS_3$. The infrared reflection spectra of the manganese-containing compounds are also included. The polarized Raman spectra (α_{zz} and α_{xx} or α_{yy} components) obtained from oriented single crystals are shown in Fig. 2. All corresponding band wavenumbers and proposed assignments are reported in Table I.

One notes many analogies between the spectra of the parent $M^{II}PS_3$ compounds and those of the corresponding substituted derivatives. In particular, bands due to ν(P–P), $\nu_s(PS_3)$, and $\delta_s(PS_3)$ are always observed at about 450, 376, and 310 cm^{-1}, respectively. Similarly, the main group frequencies related to $\nu_d(PS_3)$, $\delta_d(PS_3)$,

TABLE I

INFRARED AND RAMAN BAND WAVENUMBERS (cm^{-1}) AND ASSIGNMENTS FOR THE $MnPS_3$, $Mn_{0.87}Cu_{0.26}PS_3$, $Mn_{0.5}Ag_{1.0}PS_3$, $CdPS_3$, $Cd_{0.87}Cu_{0.26}PS_3$, AND $Cd_{0.5}Ag_{1.0}PS_3$ COMPOUNDS

$MnPS_3$		$Mn_{0.87}Cu_{0.26}PS_3$		$Mn_{0.5}Ag_{1.0}PS_3$		$CdPS_3$		$Cd_{0.87}Cu_{0.26}PS_3$		$Cd_{0.5}Ag_{1.0}PS_3$		
IR	R	IR	R	IR	R	IR	R	IR	R	IR	R	Assignments
—	—	580 sh	577 w	575 sh	—	—	—	577 sh	—	—	—	
572 vs	579 m	573 vs	571 m	568 vs	567 m	564 vs	562 m	560 vs	560 m	562 vs	562 m	
—	566 w	564 vs	562 w	558 vs	560 m	—	—	546 sh	553 sh	—	550 m	$\nu_d(PS_3)$
—	—	—	—	—	553 m	—	—	—	—	—	—	
450 m	—	449 w	—	447 w	—	449 w	—	450 w	—	448 w	—	ν(P–P)
—	382 vs	375 w	382 vs	—	372 vs	—	376 vs	370 vw	378 vs	—	370 vs	$\nu_s(PS_3)$
316 m	—	315 m	307 w	311 sh	—	310 w	298 vw	308 m	305 vw	305 sh	—	$\delta_s(PS_3)$
—	—	—	—	—	319 sh	—	—	—	—	—	—	
—	—	—	319 m	—	306 s	—	—	—	313 w	—	302 m	
—	—	323 sh	—	292 s	294 sh	—	—	300 sh	302 sh	290 m	—	
—	—	289 vw	281 sh	—	—	—	—	—	—	—	—	$\delta_d(PS)_3$
—	273 vs	266 vw	271 s	—	—	279 vw	271 s	265 sh	271 m	—	—	
255 s	—	254 s	—	—	—	252 s	—	250 s	—	—	—	
—	—	250 sh	—	—	—	—	—	—	—	—	—	
—	244 vs	—	243 s	—	246 m	—	248 vs	—	247 vs	—	248 m	
—	225 m	225 w	222 m	211 m	210 m	—	230 m	220 w	219 m	207 w	210 w	$T'_{xy}(PS_3)$
—	220 sh	—	211 sh	—	200 m	—	214 sh	200 sh	203 sh	—	192 m	
194 s	185 vw	193 s	192 vw	182 s	184 sh	193 s	—	188 s	190 sh	173 m	—	
152 s	154 m	156 s	154 w	—	160 vw	—	—	155 sh	—	—	—	$R'_{xy}(PS_3)$
138 s	—	140 w	142 w	132 m	133 w	120 s	125 m	125 sh	129 w	122 m	125 w	T'_z(Mn, Cd)
115 vw	115 w	110 vw	116 vw	—	—	100 s	110 w	112 s	110 vw	106 sh	108 w	
—	110 w	98 w	104 vw	95 m	97 w	—	—	84 s	—	—	—	
—	—	—	—	—	—	—	77 s	68 sh	66 m	72,5 m 67,5 m	—	T'_{xy}(Mn, Cd)
—	—	—	75 vw	48 w	51 w	—	—	—	77 w	45 w	46 w	T'_{xy}(Cu, Ag)
—	—	52 vw	57 m	32 m	31 s	—	—	—	56 w	30 w	31 s	
—	—	45 w	46 m	—	—	—	—	—	48 sh	—	—	T'_z(Cu, Ag)
—	—	—	37 sh	—	23 s	—	—	—	—	—	21 s	T'_{xy}(Ag)

Note. ν, stretch; δ, deformation; T', translation; R', rotation; vs, very strong; s, strong; m, medium; w, weak; vw, very weak; sh, shoulder.

$R'_{xy}(PS_3)$, $T'(PS_3)$, and $T'(M^{II})$ modes can be straightforwardly recognized. This shows that the layered frameworks built up from P_2S_6 entities are maintained in these new compounds as first demonstrated for $Mn_{0.87}Cu_{0.26}PS_3$ (*14, 15*). In the same way, the Raman spectra of the various lattices exhibit quite similar polarization effects (Fig. 2) and, as a general rule, the polarizability components α_{xx} and α_{yy} give rise to identical spectra. Such an isotropy in the **a** and **b** directions confirms the bidimensional structure of these lattices; the layers thus result from the juxtaposition of P_2S_6 (33%), $M^{II}S_6$ [$(2(1 - x)/3)$%] and $(M^I_2)S_6$ [$(2x/3)$%] pseudooctahedra and the monometallic and bimetallic sites are expected to be quite different (Fig. 3).

Despite the above-mentioned analogies, several significant spectral changes allow us to differentiate not only the $M^{II}PS_3$ and $M^{II}_{1-x}M^{I}_{2x}PS_3$ families but also the copper- and silver-containing compounds. The predominant features are the very low frequency signals ($\nu < 75$ cm^{-1}), strongly metal dependent and thus assigned to $T'(M^I)$ modes, and also the splitting of the $\nu_d(PS_3)$ and $\delta_d(PS_3)$ vibrations which confirms the existence of distorted P_2S_6 groups. In fact, as shown in Fig. 3, the change in the

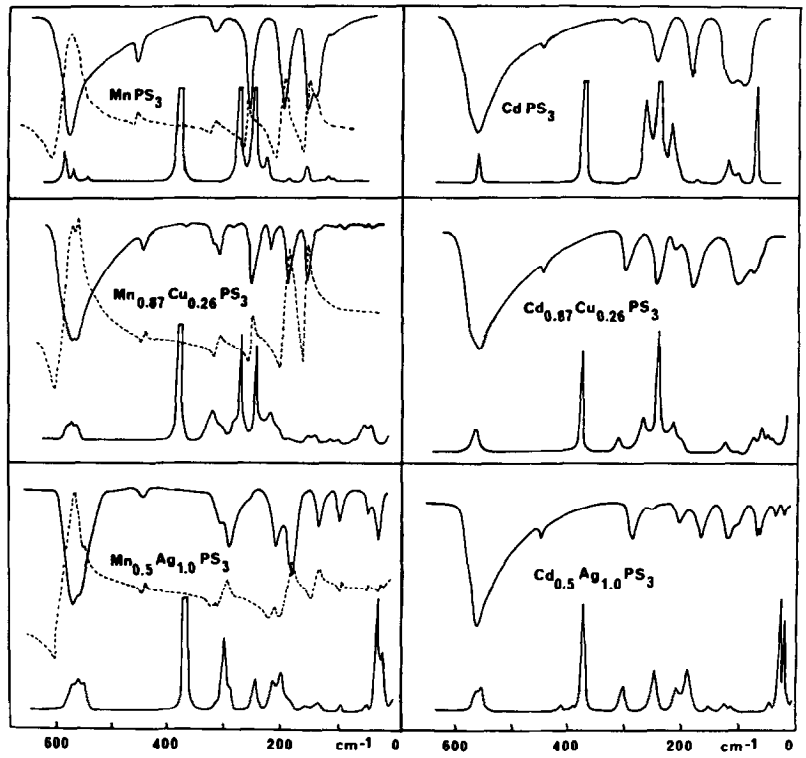

FIG. 1. Vibrational spectra (650–10 cm^{-1}) of $MnPS_3$, $Mn_{0.87}Cu_{0.26}PS_3$, $Mn_{0.5}Ag_{1.0}PS_3$, $CdPS_3$, $Cd_{0.87}Cu_{0.26}PS_3$, and $Cd_{0.5}Ag_{1.0}PS_3$ polycrystalline samples. Solid line, IR absorption and Raman spectra at 300 K; dashed line, reflection spectra at 300 K.

center-to-apex distances on going from the $Mn^{II}S_6$ octahedron (2.61 Å) to the $(Cu^I)_2S_6$ one (2.83 Å) clearly indicates the presence of strong distortions within the layers. Moreover, comparison of the ionic radii of Cu^I (0.96 Å) and Ag^I (1.26 Å) and of the substitution rates in the copper ($x = 0.13$) and silver ($x = 0.50$) derivatives shows that the silver lattices must be markedly perturbed. In fact, the spectra of the silver systems display modifications more pronounced than those observed for the copper compounds, but these effects still cannot be compared with the drastic intensity and frequency changes reported for $Cr^{III}_{0.5}Ag^I_{0.5}PS_3$ and due to the presence of (Ag^IS_6) chain-like units (*21*). This definitely corroborates the existence of $(Ag^I)_2S_6$ bimetallic entities in the $M^{II}_{0.5}Ag^I_{1.0}PS_3$ systems. As comparable vibrational spectra are observed for the two copper derivatives on the one hand and for the two silver compounds on the other, we now examine successively these two classes.

$Mn_{0.87}Cu_{0.26}PS_3$ and $Cd_{0.87}Cu_{0.26}PS_3$. Figure 4 presents the infrared reflection spectra of the two copper compounds, obtained from pressed pellets and from monocrystalline platelets. The corresponding absorption spectra of $Mn_{0.87}Cu_{0.26}PS_3$ are also included; band saturations are due to the excessive thickness of the available platelet. Since the infrared and Raman spectra compare nicely with those of the $M^{II}PS_3$ phases, assignments have been straightforwardly established with confidence (Table

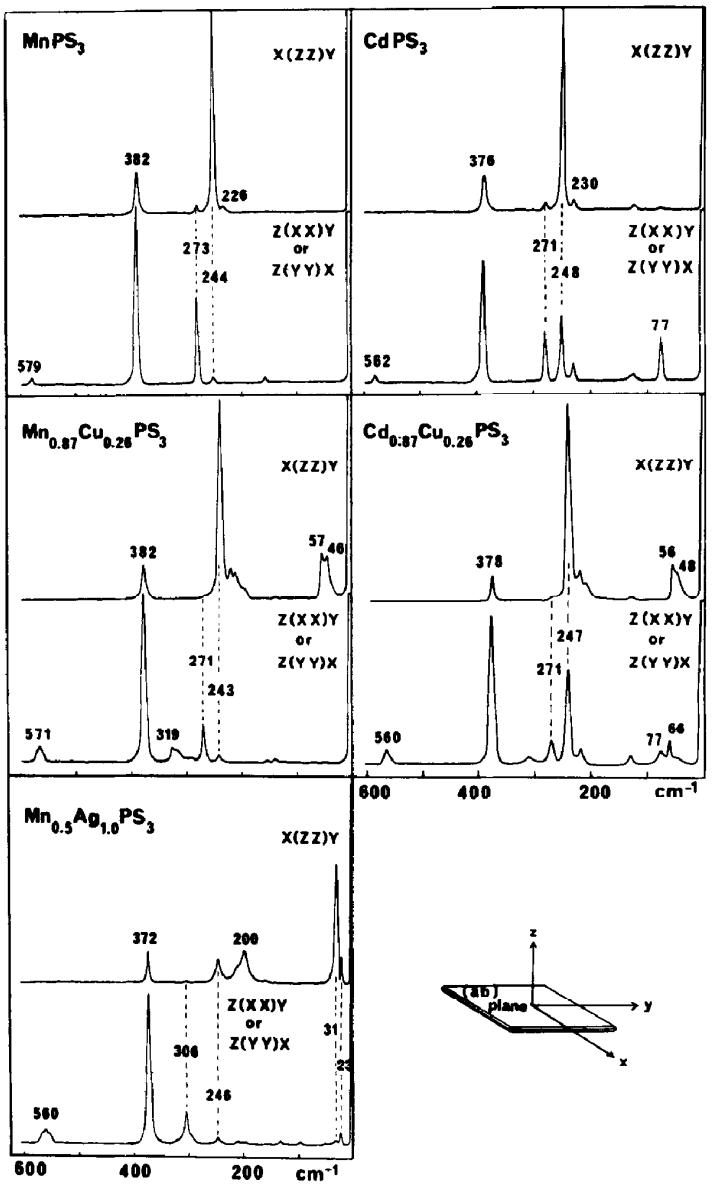

FIG. 2. Raman spectra (600–10 cm^{-1}) of monocrystalline platelets, in the (*zz*) and the (*xx*) or (*yy*) configurations, for $MnPS_3$, $Mn_{0.87}Cu_{0.26}PS_3$, $Mn_{0.5}Ag_{1.0}PS_3$, $CdPS_3$, and $Cd_{0.87}Cu_{0.26}PS_3$ compounds at 300 K. Inset: orientation of the crystal layer plane (*ab*) with respect to the *x*, *y*, and *z* directions.

I); however, one notes new vibrational components and some infrared Raman coincidences indicating a relaxation of the selection rules on going from $M^{II}PS_3$ to $M^{II}_{0.87}Cu^{I}_{0.26}PS_3$. This is a direct consequence of the structural disorder induced in these lattices by a random distribution of 13% $(Cu)_2$ pairs among the metallic sites (*14*). Moreover, the distortion of P_2S_6 groups is evidenced mainly by the activity of new "in-plane" polarized infrared and Raman $\delta(PS_3)$ components at 305–315 cm^{-1} and by

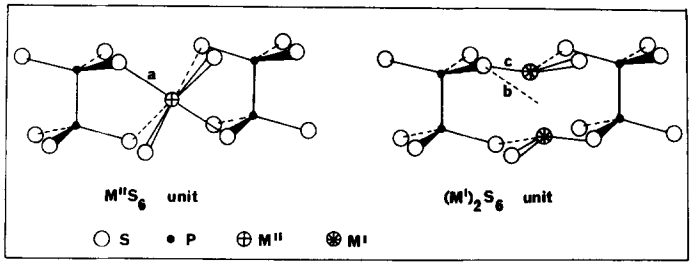

FIG. 3. Schematic representation of the M^{II} and M^I sites in $M^{II}_{1-x}M^I_{2x}PS_3$ compounds. Characteristic distances in $Mn_{0.87}Cu_{0.26}PS_3$ [from Ref. (*14*)] are a = 2.61 Å, b = 2.83 Å, c = 2.22 Å.

the intensity decrease of the Raman line at 270 cm^{-1}. Analyses of less substituted copper phases ($0 < x < 0.13$) indicate that these intensity changes increase with the Cu^I ionic content although the frequencies do not shift: we thus assign the new bands at 305–315 cm^{-1} to deformations of PS_3 units located in the vicinity of a $(Cu)_2$ entity; the 40 cm^{-1} frequency shift underlines the existence of higher constraints in the surrounding of the $(Cu^I)_2S_6$ pseudooctahedra.

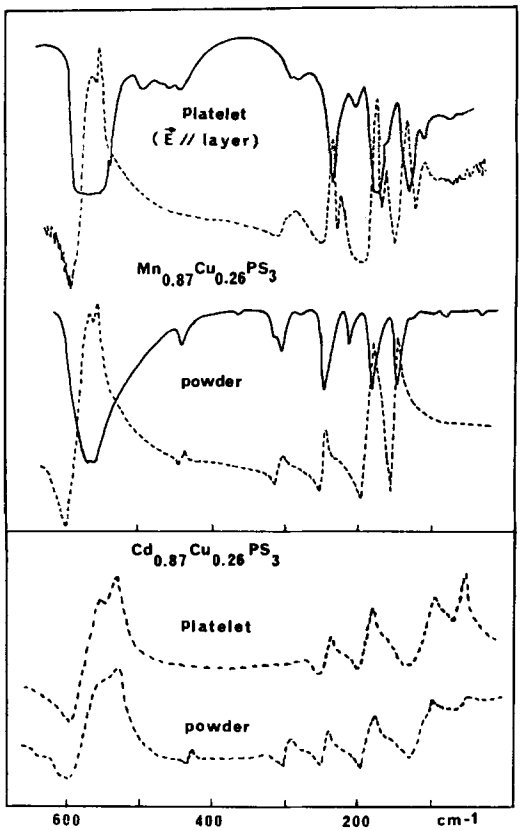

FIG. 4. Infrared spectra (650–30 cm^{-1}) of $Mn_{0.87}Cu_{0.26}PS_3$ and $Cd_{0.87}Cu_{0.26}PS_3$ polycrystalline samples and monocrystalline platelets (**E** // layer plane) at 300 K. Solid line, absorption spectra; dashed line, reflection spectra.

As expected, the infrared bands at 450 and 380 cm^{-1} due to ν(P–P) and $\delta_s(PS_3)$ out-of-plane vibrations in $Cd_{0.87}Cu_{0.26}PS_3$ nearly disappear in the spectra of platelets (**E** parallel to layer planes). Such behavior has already been reported for $CdPS_3$ (*16*) and $MnPS_3$ (*20*) single crystals. Similar polarization effects seem to take place in $Mn_{0.87}Cu_{0.26}PS_3$ but the results are more complex due to the presence of overtones in the 460–540 and 300–330 cm^{-1} regions (thick platelet).

In the low-frequency region, the "in-plane" translation modes (T'_{xy}) of the Mn^{II} and Cd^{II} ions are detected in the 130–66 cm^{-1} range but no information concerning the $T'_z(M^{II})$ and $T'_i(M^I)$ vibrations is obtained from the infrared spectra. In contrast, these vibrations can be assigned from the Raman (Fig. 2) and inelastic neutron scattering results (Fig. 5). The low-frequency Raman spectra of both copper compounds exhibit two intense signals at 55.5 ± 1.0 and 47.0 ± 1.0 cm^{-1} in the α_{zz} configuration, with intensities increasing with the substitution rate (x). Assuming that they are not markedly coupled with any other lattice mode, we assign them to $T'_z(Cu^I)$ "out-of-plane" translations. The

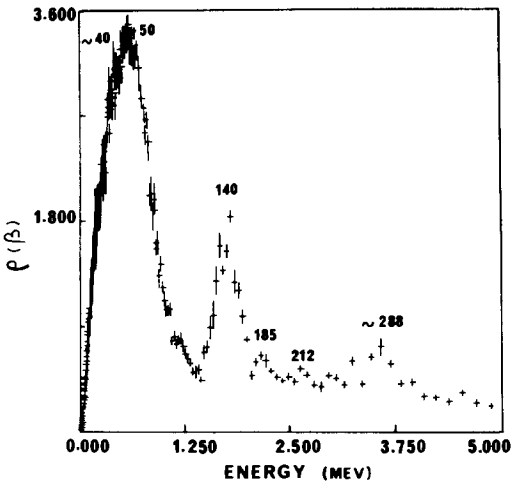

FIG. 5. INS spectrum of $Mn_{0.87}Cu_{0.26}PS_3$ at 520 K in the low-transfer-energy region (band wavenumbers are indicated in cm^{-1}).

close analogies in frequencies, band contours, polarization properties, and temperature dependence of these signals in both copper phases confirm that $(Cu^I)_2$ pairs do exist in $Cd_{0.87}Cu_{0.26}PS_3$ as in $Mn_{0.87}Cu_{0.26}PS_3$. Under these conditions the remaining two peaks at 78 and 66 cm^{-1} in $Cd_{0.87}Cu_{0.26}PS_3$ (α_{xx} or α_{yy}) are probably due to T'_{xy} modes. The more intense and sharp band at 66 cm^{-1} probably corresponds to the $T'_{xy}(Cd^{II})$ mode observed at 77 cm^{-1} in $CdPS_3$; meanwhile we propose to associate the broad signal at 78 cm^{-1} to the $T'_{xy}(Cu^I)$ vibration.

Finally, the INS spectrum of $Mn_{0.87}Cu_{0.26}PS_3$ exhibits a very intense broad signal centered at ~50 cm^{-1} and a medium intensity band at ~140 cm^{-1}, indicating that low-frequency modes involving the metal ions lead to large-amplitude motions (Fig. 5). Although we are not dealing with a system possessing large incoherent neutron scattering ionic cross sections ($\sigma_{inc}^{Cu} = 0.52 \times 10^{-24}$ cm^2 and $\sigma_{inc}^{Mn} = 0.40 \times 10^{-24}$ cm^2), it is noteworthy that the high flux available on the IN6 instrument has allowed us to obtain reasonable statistics after a beam time exposure of a few hours. The former INS signal thus corresponds to $T'_z(Cu^I)$ vibrations and the latter one is likely due to a $T'_z(Mn^{II})$ mode. In fact, the Cu^I ions and, to a lesser extent, the Mn^{II} ions have been shown to present large anisotropic thermal factors in the direction perpendicular to the layer planes (*14*). This point of great interest for the ionic transport properties of this material at high temperature is developed in Part II of this study (*22*).

$Mn_{0.5}Ag_{1.0}PS_3$ and $Cd_{0.5}Ag_{1.0}PS_3$. In contrast with the above results, the silver derivative spectra are significantly perturbed. As noted earlier, this results probably from the high degree of substitution ($x = 0.5$) and the steric hindrance of the $(Ag^I)_2$ pairs in these lattices. The $\delta_d(PS_3)$ components observed at 270–250 cm^{-1} in $M^{II}PS_3$ and split over the wide 320–250 cm^{-1} region in the copper systems appear now at 306 cm^{-1} (Raman) and 290 cm^{-1} (infrared). This suggests that all the P_2S_6 units are similarly perturbed and that an ordered distribution of the P_2S_6, $M^{II}S_6$, and $(Ag^I)_2S_6$ entities takes place, each occupying one-third of the intralamellar sites. In support of this assumption, we note a decrease in the band multiplicity on the spectra of the silver compounds (Table I) which probably indicates a higher structural ordering.

In the low-frequency region, two intense Raman peaks are observed at 31 ± 1 and 22 ± 1 cm^{-1} which are confidently assigned to translational modes of Ag^I ions. As shown in Fig. 2 (see $Mn_{0.5}Ag_{1.0}PS_3$), the former signal is due to a large contribution of the α_{zz} polarizability component and it is assigned to a $T'_z(Ag^I)$ motion; this mode leads presumably to large vibrational amplitudes of the silver ions. The later Raman signal is not totally polarized and it may correspond to $T'_{xy}(Ag^I)$ modes as well as a weak line at 51 cm^{-1}. Although no polarization data were obtained for the last compound, $Cd_{0.5}Ag_{1.0}PS_3$, similar assignments are proposed and reported in Table I.

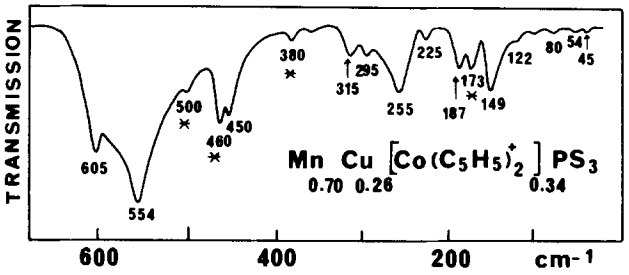

FIG. 6. Infrared spectrum (650–30 cm^{-1}) of the $Mn_{0.70}Cu_{0.26}[Co(C_5H_5)_2^+]_{0.34}PS_3$ system at 300 K. Asterisks indicate bands due to internal vibrations of $Co(C_5H_5)_2^+$.

Vibrational Spectra and Magnetic Properties of $Mn_{0.87}Cu_{0.26}PS_3$ Intercalated with $Co(C_5H_5)_2^+$

Attempts to intercalate $Co(C_5H_5)_2^+$ within the gaps of the substituted phase $Mn_{0.87}Cu_{0.26}PS_3$ proved successful under conditions similar to those previously used for intercalation in $MnPS_3$ (*23*). After complete reaction, we thus obtained $Mn_{0.70}Cu_{0.26}PS_3$, $[Co(C_5H_5)_2]_{0.34}$. Hence, the intercalation mechanism involves the departure of Mn^{2+} ions and the subsequent creation of intralayer vacancies; no exchange of Cu^I ions is observed and the degree of intercalation ($y = 0.34$) compares nicely to that reported in various MPS_3 systems (*15, 17, 29*) intercalated with this organometallic cation (0.33 ± 0.05). Therefore, as demonstrated previously (*30*), this concentration is determined mainly by the size of the guest species and the reaction is likely to be limited by the maximum filling of one layer of the intercalated species in the gap area. This shows that the $Mn_{0.87}Cu_{0.26}PS_3$ phase is a new bidimensional host lattice able to intercalate guest molecules or ions.

The infrared spectrum of this intercalated compound is shown in Fig. 6. No Raman spectrum has been obtained as the sample is a strongly absorbing material and decomposes rapidly under laser irradiation. At first glance, the infrared spectrum is a juxtaposition of bands due to the guest cation and to the host lattice. Actually, the former ones are characteristic of internal modes in $Co(C_5H_5)_2^+$ and their band wavenumbers are similar to those known in halide salts (*31*). Weak perturbations of the lattice bands with respect to the spectrum of the unintercalated phase appear as in the $MnPS_3$ intercalates (*15*). The main feature is the splitting of the broadband centered at 570 cm^{-1} into two groups of absorptions at 605 and 554 cm^{-1} which underlines the existence of structural distortions and perhaps the formation of a superstructure upon intercalation (*15, 17*). These results are consistent with the presence of disorder in the Mn^{II} surroundings and they agree with the magnetic properties (see below). Finally, it is worthwhile to note that the weak signals at 45 and 54 cm^{-1} can be related to those at 45 and 52 cm^{-1} in the starting host lattice (Table I and assigned to $T_2'(Cu^I)$ motions. The absence of frequency changes in the low-frequency region suggests that the surroundings of the copper ions are not markedly perturbed upon intercalation.

The variations of reciprocal magnetic susceptibilities as a function of temperature for $Mn_{0.87}Cu_{0.26}PS_3$ and its intercalated phase are reported in Fig. 7 (traces b and d) and are compared with those of $MnPS_3$ (trace a) and $Mn_{0.83}PS_3[Co(C_5H_5)_2]_{0.34}$ (trace c) (*27, 28*). This analysis has led us to distinguish between the high-temperature range ($T > 60$ K) and the low-temperature range (below 60 K).

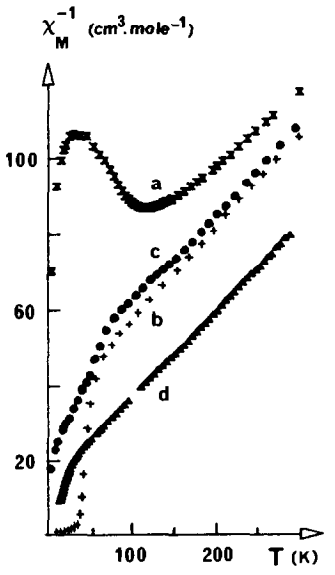

FIG. 7. Experimental reciprocal magnetic susceptibility versus temperature for (×) $MnPS_3$, (●) $Mn_{0.87}Cu_{0.26}PS_3$, (+) $Mn_{0.83}PS_3[Co(C_5H_5)_2^+]_{0.34}$, and (▲) $Mn_{0.70}Cu_{0.26}PS_3[Co(C_5H_5)_2^+]_{0.34}$.

The upper parts of traces b and c are almost linear. They have been unambiguously ascribed to the paramagnetic behavior of antiferromagnetically interacting Mn^{2+} ions in the layers (*15, 27, 28*). Upon comparing the corresponding χ values with those registered for the reference compound $MnPS_3$ (trace a) it appears that substitution and intercalation have both induced an important reduction of the antiferromagnetic coupling experimented by the intralamellar Mn^{2+}. At first glance, it seemed tempting to associate the almost coincident χ^{-1} values observed for the two $MnPS_3$-related systems (b and c) with the rather close values of the Mn coefficients in their formula unit. In fact, one may expect that the exchange coupling parameter and the χ^{-1} values decrease when the amount of Mn^{2+} vacancies increases. This trend is confirmed by the much lower χ^{-1} values obtained with the intercalated substituted system (d). Nevertheless, previous magnetic studies have shown that no quantitative relationship holds between the lowering of the magnetic interaction and the amount of Mn^{2+} in the layer (*27, 32*). In fact, while EXAFS spectroscopy has revealed the existence of a noticeable local disorder around the Mn^{2+} centers in intercalated $MnPS_3$ systems (*31, 32*), no similar observation was made for the (MnS_6) sites in the substituted compound $Mn_{0.87}Cu_{0.26}PS_3$ (*15*). Hence, in this last system, the spin dilution induced by the random distribution of 0.13 (Cu_2S_6) entities among 0.87 unchanged (MnS_6) units appears to be the only important factor responsible for reduction of the coupling. Such dilution effect exists in $Mn_{0.83}PS_3[Co(C_5H_5)_2]_{0.34}$, but the presence of metal vacancies also induces lattice distortions, with various slightly different (MnS_6) orientations, and thus leads to additional modifications of the exchange pathway, which is known to be extremely sensitive to the local symmetry. Therefore, the quasi-coincidence of the high-temperature behavior of traces b and c cannot be explained directly from stoichiometric considerations.

Trace d presents a linear shape with a slope comparable to those of traces a, b, and c, still characteristic of an antiferromagnetic exchange coupling. Both spin dilution and canting effects, resulting from metal substitution and metal vacancies, again contribute to considerably reduce the coupling constant. Obviously, the $Mn_{0.70}Cu_{0.26}PS_3[Co(C_5H_5)_2]_{0.34}$ compound has almost reached the percolation limit beyond which the remaining Mn^{2+} behave as uncoupled paramagnetic ($S = \frac{5}{2}$) centers.

Consider now the low-temperature range: the magnetic behavior of the intercalated system (c) undergoes an abrupt transition which has been shown to indicate the rapid onset of a weak ferromagnetism phenomenon among the locally disordered intralayer manganese (*26, 27*). The χ^{-1} trace of the substituted system (b) shows a weaker but still significant discontinuity

around 75 K. Since no suggestion of manganese ion disorder can be invoked in this case (*15*), we propose to interpret this low-amplitude transition as resulting from a weak ordering ferromagnetic phenomenon taking place among the stacked two-dimensional layers. As expected, this ordering phenomenon disappears after intercalation of bulky cobalticenium cations (see trace d). Finally, the reciprocal susceptibility of $Mn_{0.70}Cu_{0.26}PS_3[Co(C_5H_5)_2]_{0.34}$ drops rapidly below 30 K; this transition is now confidently ascribed to the intercalation-induced spin canting in this structure. As noted previously (*32*), comparison of traces c and d indicates that the transition temperature decreases when the amount of Mn^{2+} vacancies increases.

Acknowledgment

The authors thank Dr. J. Grimblot for XPS and Auger measurements on $Mn_{0.87}Cu_{0.26}PS_3$.

References

1. R. Clement and M. L. H. Green, *J. Chem. Soc. Dalton Trans.* **10,** 1566 (1979).
2. M. S. Whittingham and A. J. Jacobsen, "Intercalation Chemistry," Academic Press, New York (1981).
3. R. Brec, D. M. Schleich, G. Ouvrard, A. Louisy, and J. Rouxel, *Inorg. Chem.* **18,** 1814 (1979).
4. C. D. Carpentier and R. Nitsche, *Mater. Res. Bull.* **9,** 1097 (1974).
5. A. Le Mehaute, G. Ouvrard, R. Brec, and J. Rouxel, *Mater. Res. Bull.* **12,** 1151 (1977).
6. G. Le Flem, R. Brec, G. Ouvrard, A. Louisy, and P. Segrasan, *J. Phys. Chem. Solids* **43,** 455 (1982).
7. W. Klingen, G. Eulenberger, and H. Hahn, *Z. Anorg. Allg. Chem.* **401,** 97 (1973).
8. G. Ouvrard, R. Brec, and J. Rouxel, *Mater. Res. Bull.* **20,** 1181 (1985).
9. R. Brec, G. Ouvrard, and J. Rouxel, *Mater. Res. Bull.* **20,** 1257 (1985).
10. E. Prouzet, G. Ouvrard, and R. Brec, *Mater. Res. Bull.* **21,** 195 (1986).
11. G. Ouvrard, R. Freour, R. Brec, and J. Rouxel, *Mater. Res. Bull.*, in press.
12. J. Covino, P. Dragovich, C. K. Lowe-Ma, R. F. Kubin, and R. W. Schwartz, *Mater. Res. Bull.* **20,** 1099 (1985).
13. E. Lifshitz, A. H. Francis, and R. Clarke, *Solid State Commun.* **45,** 273 (1983).
14. Y. Mathey, R. Clement, J. P. Audiere, O. Poizat, and C. Sourisseau, *Solid State Ionics* **9/10,** 459 (1983).
15. Y. Mathey, A. Michalowicz, P. Toffoli, and G. Vlaic, *Inorg. Chem.* **23,** 897 (1984).
16. Y. Mathey, R. Clement, C. Sourisseau, and G. Lucazeau, *Inorg. Chem.* **19,** 2773 (1980).
17. M. Barj, G. Lucazeau, and R. Clement, *J. Mol. Struct.* **79,** 329 (1982).
18. C. Sourisseau, J. P. Forgerit, and Y. Mathey, *J. Solid State Chem.* **49,** 134 (1983).
19. G. Kliche, *Z. Naturforsch. A* **38,** 1133 (1983).
20. G. Kliche, *J. Solid State Chem.* **51,** 118 (1984).
21. O. Poizat and C. Sourisseau, *J. Solid State Chem.* **59,** 371 (1985) and references therein.
22. O. Poizat, F. Fillaux, and C. Sourisseau, *J. Solid State Chem.* **72,** 3962 (1988).
23. R. Clement, *J. Chem. Soc. Chem. Commun.*, 647 (1980).
24. G. Narletta, O. Puglisi, S. Pignataro, G. Alberti, and U. Costantino, *Chem. Phys. Lett.* **89,** 333 (1982).
25. A. J. Dianoux, R. E. Ghosh, H. Hervet, and R. E. Lechner, ILL Internal Technical Report 75D, 16T (1975).
26. P. E. Egelstaff, *Nucl. Sci. Eng.* **12,** 250 (1962).
27. R. Clement, J. J. Girerd, and I. Morgenstern-Badarau, *Inorg. Chem.* **19,** 2852 (1980).
28. R. Clement, J. P. Audiere, and J. P. Renard, *Rev. Chim. Min.* **19,** 560 (1982).
29. C. Sourisseau, J. P. Forgerit, and Y. Mathey, *J. Phys. Chem. Solids* **44,** 119 (1983).
30. O. Poizat, C. Sourisseau, and Y. Mathey, *J. Chem. Soc. Faraday Trans. 1* **80,** 3257 (1984).
31. E. Maslowsky, *in* "Vibrational Spectra of Organometallic Compounds," Wiley, New York (1977).
32. A. Michalowicz and R. Clement, *Inorg. Chem.* **21,** 3872 (1982).